Acta Oceanol. Sin., 2021, Vol. 40, No. 1, P. 43–53
https://doi.org/10.1007/s13131-021-1717-2
http://www.hyxb.org.cn
E-mail: hyxbe@263.net

Cross-calibration of brightness temperature obtained by FY-3B/MWRI using Aqua/AMSR-E data for snow depth retrieval in the Arctic

Haihua Chen[1], Lele Li[1], Lei Guan[1]*

[1] College of Information Science and Engineering, Ocean University of China, Qingdao 266100, China

Received 25 September 2020; accepted 22 October 2020

Abstract

This study cross-calibrated the brightness temperatures observed in the Arctic by using the FY-3B/MWRI L1 and the Aqua/AMSR-E L2A. The monthly parameters of the cross-calibration were determined and evaluated using robust linear regression. The snow depth in case of seasonal ice was calculated by using parameters of the cross-calibration of data from the MWRI T_b. The correlation coefficients of the H/V polarization among all channels T_b of the two sensors were higher than 0.97. The parameters of the monthly cross-calibration were useful for the snow depth retrieval using the MWRI. Data from the MWRI T_b were cross-calibrated to the AMSR-E baseline. Biases in the data of the two sensors were optimized to approximately 0 K through the cross-calibration, the standard deviations decreased significantly in the range of 1.32 K to 2.57 K, and the correlation coefficients were as high as 99%. An analysis of the statistical distributions of the histograms before and after cross-calibration indicated that the FY-3B/MWRI T_b data had been well calibrated. Furthermore, the results of the cross-calibration were evaluated by data on the daily average T_b at 18.7 GHz, 23.8 GHz, and 36.5 GHz (V polarization), and at 89 GHz (H/V polarization), and were applied to the snow depths retrieval in the Arctic. The parameters of monthly cross-calibration were found to be effective in terms of correcting the daily average T_b. The results of the snow depths were compared with those of the calibrated MWRI and AMSR-E products. Biases of 0.18 cm to 0.38 cm were observed in the monthly snow depths, with the standard deviations ranging from 4.19 cm to 4.80 cm.

Key words: FY-3B, AMSR-E, brightness temperature (T_b), cross-calibration, snow depth, Arctic

Citation: Chen Haihua, Li Lele, Guan Lei. 2021. Cross-calibration of brightness temperature obtained by FY-3B/MWRI using Aqua/AMSR-E data for snow depth retrieval in the Arctic. Acta Oceanologica Sinica, 40(1): 43–53, doi: 10.1007/s13131-021-1717-2

1 Introduction

The climate system of the Arctic has changed dramatically in recent decades, with a rapid decrease in both the coverage and thickness of sea ice (Cavalieri et al., 2003, 2012; Cavalieri and Parkinson, 2012; Parkinson and Cavalieri, 2008; Comiso et al., 2008; Maslowski et al., 2012). These changes have had significant impacts on the global climate system, environmental systems and ecosystems across the world in general. Remote sensing technology provides a convenient means of making global observations and measurements of the ocean to research changes occurring in high-latitude regions. Passive microwave remote sensing, in particular, has been widely used in studies on the polar regions because of its all-weather and all-day detection capabilities (Comiso et al., 2003; Nihashi et al., 2009; Spreen et al., 2008).

The Advanced Microwave Scanning Radiometer for the Earth Observing System (AMSR-E) on board Aqua satellite of National Aeronautics and Space Administration (NASA) was launched in May 2002. Compared with the Scanning Multichannel Microwave Radiometer (SMMR), the Special Sensor Microwave Imager (SSMI), the Tropical Rainfall Measuring Mission (TRMM), and other microwave sensors, the AMSR-E has the advantages of multiple channels, a wider range of frequencies, and higher resolution. The T_b data of the AMSR-E have been widely used for the inversion of the parameters of sea ice and snow in the polar region (Comiso et al., 2003; Kelly et al., 2003; Markus and Cavalieri, 2008; Nihashi et al., 2009; Spreen et al., 2008). However, in October 2011, NASA's AMSR-E sensor ceased operation following instrument failure.

The Fengyun-3 (FY-3) is the second generation of China's polar-orbiting meteorological satellites. Since 2008, the National Satellite Meteorological Center has provided microwave radiation imager (MWRI) data mounted on the satellites FY-3A, 3B, 3C, and 3D, which will be in use for approximately 15 years. The settings of parameters of the FY-3B/MWRI are consistent with those of the AMSR-E and AMSR2 (a continuation of AMSR-E), and can complement microwave radiometer data (Yang et al., 2011, 2012) for research on the Earth's water cycle, climate change, and weather forecasting. Space-borne passive microwave sensors are designed to operate with different instrument-related parameters, calibration systems, bands of observation frequency, durations of observation, and observational footprints, because of which deviations occur in the observed data. Therefore, the cross-calibration and evaluation of these sensors by using overlapping areas and similar instrument-related parameters is crucial for obtaining more accurate and stable long-term radiometer observations of the Arctic.

Foundation item: The National Key Research and Development Program of China under contract Nos 2019YFA0607001 and 2016YFC1402704; the Global Change Research Program of China under contract No. 2015CB9539011.

*Corresponding author, E-mail: leiguan@ouc.edu.cn

A number of studies have been conducted on the cross-calibration of microwave radiometer data. Gao et al. (2019) studied the inter-sensor calibration between the SMR and the AMSR2 to broaden the application of SMR data to the Earth's land surface. Liu et al. (2018) inter-calibrated the brightness temperatures (T_b) between the F13 SSM/I and the F17 SSMIS by using empirical relationship models during their period of overlap. Hu et al. (2016) compared the slow-speed mode L1S of the AMSR-E with values of T_b obtained by the AMSR2 at 18.7 GHz and 36.5 GHz on the surface of land. Du et al. (2014) used the double difference to calibrate the AMSR-E and the AMSR2, and Huang et al. (2013) compared the values of T_b obtained by the MWRI and the AMSR-E in the Bohai Sea and Yellow Sea in China. Das et al. (2014) evaluated and compared land data from the same eight channels of the AMSR-E and WindSat. Cavalieri and Parkinson (2012) studied cross-calibration of the values of T_b obtained from eight channels of the SSM/I (F13) and the SSMIS (F17) to obtain more general data on sea ice. Meier et al. (2011) cross-calibrated data of the SSM/I (F13) and the SSMIS (F17) at V/H 19 GHz and V 37 GHz in the Arctic and Antarctic regions. Derksen and Walker (2003) analyzed systematic deviations in the SMMR and the SSM/I (F08) for data on the land surface of North America. Stroeve et al. (1998) took data from the SSM/I (F11) as comparative data and eight typical regions in the Arctic as research area to study the cross-calibration of five channels between the SSM/I (F8) and the SSM/I (F13). Abdalati et al. (1995) compared the 37-GHz data of the SSM/I (F08) with those of SSM/I (F11), and the linear relationship between values of T_b obtained by them was established. Jezek et al. (1993) took the Antarctic ice region as research area and the SMMR as the source of comparative data. The daily observations of the SSM/I (F08) and SMMR were analyzed by means of linear regression.

Statistical cross-calibration is best suited for two instruments with collocated and near-simultaneous observations (Chander et al., 2013). The MWRI on board the FY-3B satellite has a similar instrument-related configuration to that of the AMSR-E sensor, including five channel frequency settings (10.7 GHz, 18.7 GHz, 23.8 GHz, 36.5 GHz, and 89.0 GHz), dual polarization (H/V), and nearly simultaneous satellite overpass times. This study uses the statistical cross-calibration approach to compare observations of the FY-3B MWRI and the Aqua AMSR-E directly, and to evaluate the data on T_b collected by the MWRI. The cross-calibration of T_b obtained by the MWRI and AMSR-E can improve the passive microwave sensors as well as the monitoring and retrieval of the sea ice thickness and snow depth in the Arctic. Based on brightness temperatures measured by the AMSR-E from 2002 to 2011, an operational dataset on snow depth on sea ice in the Polar Regions has been released by NSIDC (National Snow and Ice Data Center). The relevant algorithm was developed using brightness temperatures of the SSM/I to calculate snow depth on sea ice in the southern ocean (Markus and Cavalieri, 1998), and then applied to the inversion of the snow depth in the Arctic. It was applied to AMSR-E data (Comiso et al., 2003) in 2003. Eight snow depth products were compared (Lu et al., 2020), including satellites, models, buoys, and the Ice Bridge project (OIB). The snow depth product based on AMSR-E data had the highest correlation with data on the thickness of snow obtained from OIB flight plan, and their RMSE value was smaller than those of the others. No operational dataset of snow depth on sea ice has been provided by the Fengyun MWRI for the Arctic. Therefore, it is important to evaluate the accuracy of calibration of the FY-3B MWRI by using the Aqua AMSR-E, a similar microwave remote sensing instrument that has been widely used and verified, to provide operational products on snow depth based especially on MWRI.

This paper describes the cross-calibration of data on T_b from the MWRI and AMSR-E in the Arctic. The statistical cross-calibration approach is used to study data on the monthly time–space overlap from the two sensors at all five frequencies (10.7 GHz, 18.7 GHz, 23.8 GHz, 36.5 GHz, and 89.0 GHz), dual polarization (H, V), and ascending and descending orbits. The parameters of the cross-calibration are then determined and evaluated by using robust linear regression. The depths of snow on seasonal ice were calculated using the results of the cross-calibration of data on T_b measured by the MWRI. The remainder of this paper is organized as follows: Section 2 introduces the research data, Section 3 describes the method of cross-calibration used and the snow depth retrieval algorithm, Section 4 analyzes the main results, and Section 5 presents our conclusions.

2 Dataset

2.1 *Observations of brightness temperature*

The cross-calibration dataset contained the brightness temperatures observed by the FY-3B/MWRI L1 and Aqua/AMSR-E L2A from November 18, 2010 to September 30, 2011. The spatial coverage of these data was north of 60°N in the Arctic. The data were downloaded from the NSMC (National Satellite Meteorological Centre, http://www.nsmc.cma.gov.cn/NSMC/) and DAAC (NASA Distributed Active Archive Center) at NSIDC (http://nsidc.org/), respectively. The main techniques and instrument-related parameters of the MWRI were consistent with those of the AMSR-E on all channels from 10.7 GHz to 89.0 GHz. The AMSR-E and MWRI were dual-polarized, and had equatorial transit times of 01:30/13:30 and 01:40/13:40 (descending/ascending), and incident angles of 55.0° and 53.5°, respectively. The main configurations of the two sensors are summarized in Table 1 (Du et al., 2014; Yang et al., 2012).

2.2 *Snow depth dataset*

To evaluate the data on T_b measured by the MWRI before and

Table 1. Comparison of AMSR-E and MWRI parameters

Parameter	Sensor									
	AMSR-E/AQUA					MWRI/FY-3B				
Band 1 GHz	10.7	18.7	23.8	36.5	89.0	10.65	18.7	23.8	36.5	89.0
Spatial resolution	51 km×29 km	27 km×16 km	32 km×18 km	14 km×8 km	6 km×4 km	51 km×85 km	30 km×50 km	27 km×45 km	18 km×30 km	9 km×15 km
Bandwidths/MHz	100	200	400	1 000	3 000	180	200	400	900	4 600
Polarization	V/H					V/H				
Equatorial time	13:30 (ascending) 01:30 (descending)					13:40 (ascending) 01:40 (descending)				
Incident angle/(°)	55.0					53.5				
Swath width/km	1 450					1 400				

after cross-calibration, the use of these data to the snow depth retrieval on seasonal sea ice in the Arctic was examined. The data on T_b were measured by V polarization channels of the MWRI at 18.7 GHz, 23.8 GHz, and 36.5 GHz, and by the H/V polarization channel at 89.0 GHz to calculate the snow depths (Comiso et al., 2003). The comparison dataset consisted of the snow depths measured by the AMSR-E Level-3 standard sea ice products provided by the National Snow and Ice Data Center.

These snow depths products from the MWRI and AMSR-E were projected on a standard polar stereographic grid, with an area identical to that for which the data were being cross-calibrated, at a spatial resolution of 12.5 km (Cavalieri et al., 2014; Markus and Cavalieri, 2008). The temporal coverage of the snow depth dataset ranged from January 1 to April 30, 2011.

3 Methods

3.1 *Cross-calibration method*

The MWRI and AMSR-E had similar physical configurations, overlap times, and study areas in this study. Therefore, robust linear fitting in the statistical regression method was used to compare and directly cross-calibrate their values of T_b.

3.1.1 *Preprocessing the brightness temperature*

Matrix data on longitude and latitude, DN data, and scan times from 10.7 GHz to 89.0 GHz were extracted from the HDF5 files of the MWRI and AMSR-E. The preprocessing of the values of T_b included data projection, quality control, land mask, sea ice boundary detection, and spatial-temporal matching.

First, the DN values were converted into values of T_b using a scale factor of 0.01 and an offset of 327.68. Values of T_b obtained by the MWRI and AMSR-E (10.7 GHz, 18.7 GHz, 23.8 GHz, 36.5 GHz, and 89.0 GHz; H and V polarization; ascending and descending orbits) were projected onto the research region using spherical polar projection (Markus and Cavalieri, 2008) provided by the NSIDC. After the projection, the data resolution was 12.5 km× 12.5 km. Second, the abnormal or erroneous data were removed in quality control. A 3 × 3 window was used as template to scan the data. If the standard deviation of the data on T_b in the template was greater than 3 K, the data in the template were removed. In addition, values of T_b greater than 320 K or less than 70 K were deleted (Li and Zhong, 2011). Third, to find the boundary between coastal water and ice water, a 7 × 7 window was selected to expand the land mask based on the land mask file from the NSIDC. The data points were marked as invalid if land points were obtained in the 7 × 7 window. In addition, using data on the V polarization of T_b at 18.7 GHz and 36.5 GHz from the MWRI, the intensity ratios and gradients were calculated to determine the threshold, 0.9, as edges of the sea ice (Svendsen et al., 1983; Zhang, 2012). Finally, a matching time window was selected in which the difference between data of the two sensors was less than 30 min, and spatial and temporal data matching between the MWRI and the AMSR-E was carried out.

3.1.2 *Cross-calibration based on robust linear regression*

After data preprocessing, the one-dimensional (1D) sequence datasets used for cross-calibration were obtained based on the matrix data on spatial and temporal matching. Because of the similar satellite-related parameters and nearly simultaneous satellite overpass times of the two radiometers, robust linear regression analysis was applied for cross-calibration according to the following equation:

$$T_{\mathrm{MWRI}} - T_{\mathrm{AMSR\text{-}E}} = a \times T_{\mathrm{AMSR\text{-}E}} + b, \tag{1}$$

where T_{MWRI} and $T_{\mathrm{AMSR\text{-}E}}$ denote data on T_b obtained from the MWRI and the AMSR-E, respectively. The parameters a and b are the slope and offset of the relationship, in terms of T_b, between the values of the AMSR-E and the MWRI minus the AMSR-E.

Therefore, the calibrated data on T_b from the MWRI were corrected using the AMSR-E baseline through the following expression:

$$T'_{\mathrm{MWRI}} = \frac{T_{\mathrm{MWRI}} - b}{a+1} = \frac{1}{a+1} T_{\mathrm{MWRI}} - \frac{b}{a+1}, \tag{2}$$

where $\frac{1}{a+1}$ is the slope and $-\frac{b}{a+1}$ the offset of the equation of the coefficient of cross-calibration between data on T_b obtained from the MWRI and AMSR-E.

3.2 *Snow depth retrieval algorithm*

According to the concentration of sea ice, and the proportional relationship between snow depth and surface scattering, snow depth was calculated by the AMSR-E algorithm (Kelly et al., 2003; Comiso et al., 2003). The data on T_b at 36.5 GHz and 18.7 GHz (V polarization) were used to derive the snow depths on seasonal sea ice (Comiso et al., 2003). The relevant equations are as follows:

$$h_s = 2.9 - 782.4 \times \mathrm{GRV}, \tag{3}$$

$$\mathrm{GRV} = \frac{T_b(36.5\mathrm{V}) - T_b(18.7\mathrm{V}) - k_1(1-C)}{T_b(36.5\mathrm{V}) + T_b(18.7\mathrm{V}) - k_2(1-C)}, \tag{4}$$

$$k_1 = T_{b0}(36.5\mathrm{V}) - T_{bo}(18.7\mathrm{V}), \tag{5}$$

$$k_2 = T_{b0}(36.5\mathrm{V}) + T_{b0}(18.7\mathrm{V}), \tag{6}$$

where h_s is the snow depth, T_{b0} is the average value of the brightness temperature on different channels for open water, and C is the sea ice concentration.

Using the above snow depth retrieval algorithm, the daily snow depths obtained from the MWRI were calculated with the daily sea ice concentrations based on the ASI algorithm (Kaleschke et al., 2001; Spreen et al., 2008) and the brightness temperatures of the MWRI at 18.7 GHz and 36.5 GHz (V polarization). The snow depth retrieval algorithm is applicable to dry snow on seasonal ice in the Arctic. The emissivities of 18.7 GHz and 36.5 GHz are almost identical, because of which the snow depth cannot be determined for wet snow. Moreover, the algorithm can calculate only the depths greater than 50 cm because the penetration depth of microwave signals at 18.7 GHz and 36.5 GHz is less than 50 cm.

4 Results and discussion

4.1 *Analyzing results of cross-calibration*

According to the robust linear regression, the data on T_b from the MWRI and AMSR-E were cross-calibrated using the AMSR-E data as the baseline. The different periods of the matching data, including day, week, half-week and month were compared, and the month was finally selected as the unit of the matching period. A randomly selected subset (two-thirds of all matching data from all channels, polarization, and both ascending and descending

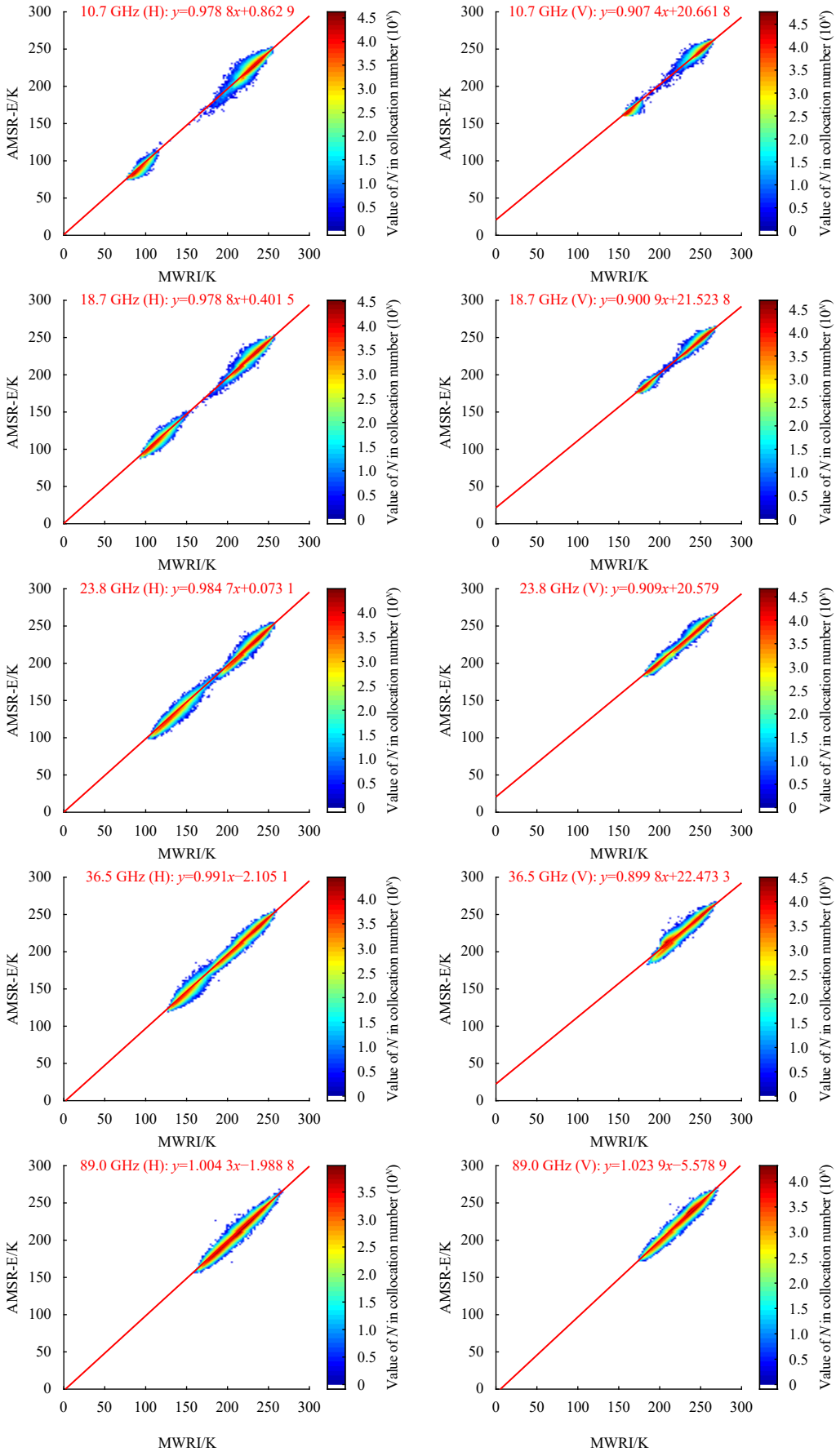

Fig. 1. Cross-calibration for 10.7–89.0 GHz (H/V polarization, ascending) in January 2011.

T_b) was used as calibration data and the remainder as test data for validation.

By taking the data in January 2011 as an example of the cross-calibration, scatter plots of the test ascending data on T_b from the MWRI and AMSR-E are shown in Fig. 1. The regression equations are given at the top of the figures. They show clear linear relationships between the MWRI and the AMSR-E data. According to the regression equations, the intercepts of the fitting lines for the V polarization were greater in number than those for the H polarization, and the slopes were at about 0.9. The results of fitting of each channel of the horizontal polarization were closer to $y=x$ than those of the vertical polarization.

Table 2 shows the statistical parameters of cross-calibration, including the mean deviation (bias), standard deviation (STD), and correlation coefficient (R) of data on the ascending and descending orbits of the 10.7–89.0 GHz V/H polarization.

Compared with the results before cross-calibration in Table 2, the biases (mean of MWRI minus AMSR-E) and standard deviations were all corrected. After cross-calibration, the average deviation of each channel was about 0 K and the values of standard deviation had decreased significantly. The biases ranged from –0.008 9 K to 0.006 9 K, the standard deviations ranged from 1.316 5 K to 2.567 2 K, and R was up to 99%. The deviations in the V polarization of data from each channel before cross-calibration were larger than those for the H polarization, and the former had been significantly corrected after calibration. The analysis shows that the MWRI data had been significantly modified.

Figure 2 shows the statistical histograms for all channels (10.7–89.0 GHz, H and V polarizations) in steps of 1 K with the entire ascending and descending orbits T_b data. The figures on the left are the distributions of statistical histogram of the data on T_b obtained by the MWRI and AMSR-E before cross-calibration, and those on the right show the statistical histogram of the two sensors after cross-calibration.

The results indicate that the data on T_b obtained by the MWRI were more consistent with those of the AMSR-E than before the cross-calibration. Cross-calibration through robust linear regression reduced deviations among the observational data between the MWRI and the AMSR-E. The variations in microwave emissivity at frequencies for one-year ice, multi-year ice, and open water for the vertical and horizontal polarizations (Svendsen et al., 1983) showed that the emissivity of the V polarization was greater than that of the H polarization. The emissivity of multi-year ice was significantly higher than that of open water. From scatters of the distribution of T_b in Fig. 1, it is clear that the range of distribution of the H polarization of the data on T_b was wider than that of the V polarization. The values of T_b for the V polarization were generally higher than those for the H polarization. The statistical histograms of data from the MWRI and the AMSR-E in Fig. 2 show a bi-modal structure, except at 89.0 GHz. In the low-frequency distributions of T_b, the bi-modal structures are evident, and reflect the characteristics of open water and sea ice.

4.2 *Results for snow depth*

The snow depth retrieval algorithm described in Section 3.2 determined the sea ice concentration and the snow depths mainly using the daily average values of T_b at frequencies of 18.7 GHz, 23.8 GHz, and 36.5 GHz (V polarization) as well as 89.0 GHz (H/V polarization). Based on the parameters of cross-calibration obtained in this study, values of the daily average T_b of the above channels were analyzed and evaluated, and snow depths using the channels data of the MWRI were further studied in the Arctic.

4.2.1 *Assessing the cross-calibration of daily average brightness temperature*

As an example, Fig. 3 shows the distributions of the daily average values of T_b at frequencies 89.0 GHz of the V polarization on January 1, 2011. The figures on the left are the results of the MWRI, and the figures on the right are those of the AMSR-E. The data show similar spatial distributions but there are deviations. The white points and areas in Fig. 3 are the outliers removed by preprocessing and areas with no observed data.

Based on the analysis in Section 4.1, the parameters of the monthly cross-calibration were used to process daily average values of T_b as obtained by the MWRI. To reduce the interference of mixed pixels, the method described in Section 3.1.1 was applied to the daily average T_b to remove pixels along the edges of the land and sea, representing ice and water, respectively. Statistical evaluations were applied to differences in the daily average T_b before and after cross-calibration from November 8, 2010 to September 30, 2011 (317 d).

Figure 4 shows the bias, standard deviation, and RMSE of the daily average T_b as obtained by the MWRI before and after cross-calibration, with the corresponding data from channels of the AMSR-E. It can be seen that the parameters of monthly cross-calibration were effective in terms of calibrating the daily T_b values of the MWRI, and deviations between the MWRI and the AMSR-E after calibration were clearly corrected.

The average bias, standard deviation, and RMSE of the daily average data on T_b for each channel are given in Table 3. The deviations after cross-calibration were corrected, and the biases ranged from –0.06 K to –0.71 K. The RMSE and STD values after

Table 2. Comparison of statistical parameters before and after the cross-calibration of matching data on values of T_b of the MWRI and AMSR-E

Channel	Before cross-calibration/after cross-calibration							
	Ascending				Descending			
	Number	Bias/K	STD/K	R	Number	Bias/K	STD/K	R
10.7 GHz (V)	27 419 394	–3.814 9/0.004 0	4.965 4/1.714 6	0.997 4/0.999 1	20 619 591	–3.731 0/–0.002 4	5.198 5/1.689 0	0.997 6/0.999 2
10.7 GHz (H)	25 560 857	–0.701 3/0.000 1	4.081 3/2.399 3	0.998 3/0.999 4	19 202 858	0.322 3/0.002 6	3.680 0/2.312 5	0.998 8/0.999 5
18.7 GHz (V)	27 905 067	–1.646 7/–0.000 9	4.009 5/1.352 1	0.997 4/0.999 1	21 042 823	–1.644 1/–0.006 3	4.126 6/1.316 5	0.997 7/0.999 2
18.7 GHz (H)	25 962 969	0.858 3/0.000 5	3.006 0/1.909 7	0.998 8/0.999 5	19 544 190	1.504 2/–0.004 9	2.895 4/1.883 1	0.999 0/0.999 5
23.8 GHz (V)	27 975 385	–3.075 7/0.000 3	3.844 0/1.669 8	0.992 7/0.997 5	21 111 826	–2.783 2/–0.000 2	3.973 3/1.624 7	0.993 3/0.997 7
23.8 GHz (H)	25 151 517	–0.164 6/–0.003 4	3.278 1/2.140 5	0.997 6/0.998 9	18 840 245	0.494 6/–0.002 3	3.240 8/2.167 5	0.997 9/0.999 0
36.5 GHz (V)	27 461 876	–2.980 8/0.001 4	5.259 5/2.246 7	0.974 6/0.992 8	20 794 592	–3.277 8/–0.003 7	5.246 0/2.127 9	0.976 9/0.992 7
36.5 GHz (H)	22 491 629	0.869 9/–0.004 6	3.317 3/2.219 8	0.996 8/0.998 5	16 585 284	1.516 8/0.000 5	3.378 8/2.259 7	0.996 9/0.998 5
89.0 GHz (V)	22 304 767	–1.424 5/0.006 9	2.694 3/2.441 5	0.988 7/0.990 4	18 163 675	–1.108 7/0.003 2	2.626 5/2.393 4	0.988 5/0.990 3
89.0 GHz (H)	15 749 987	–0.286 0/–0.000 9	2.697 6/2.531 8	0.991 9/0.993 0	11 461 719	0.082 6/–0.008 9	2.747 6/2.567 2	0.990 5/0.991 8

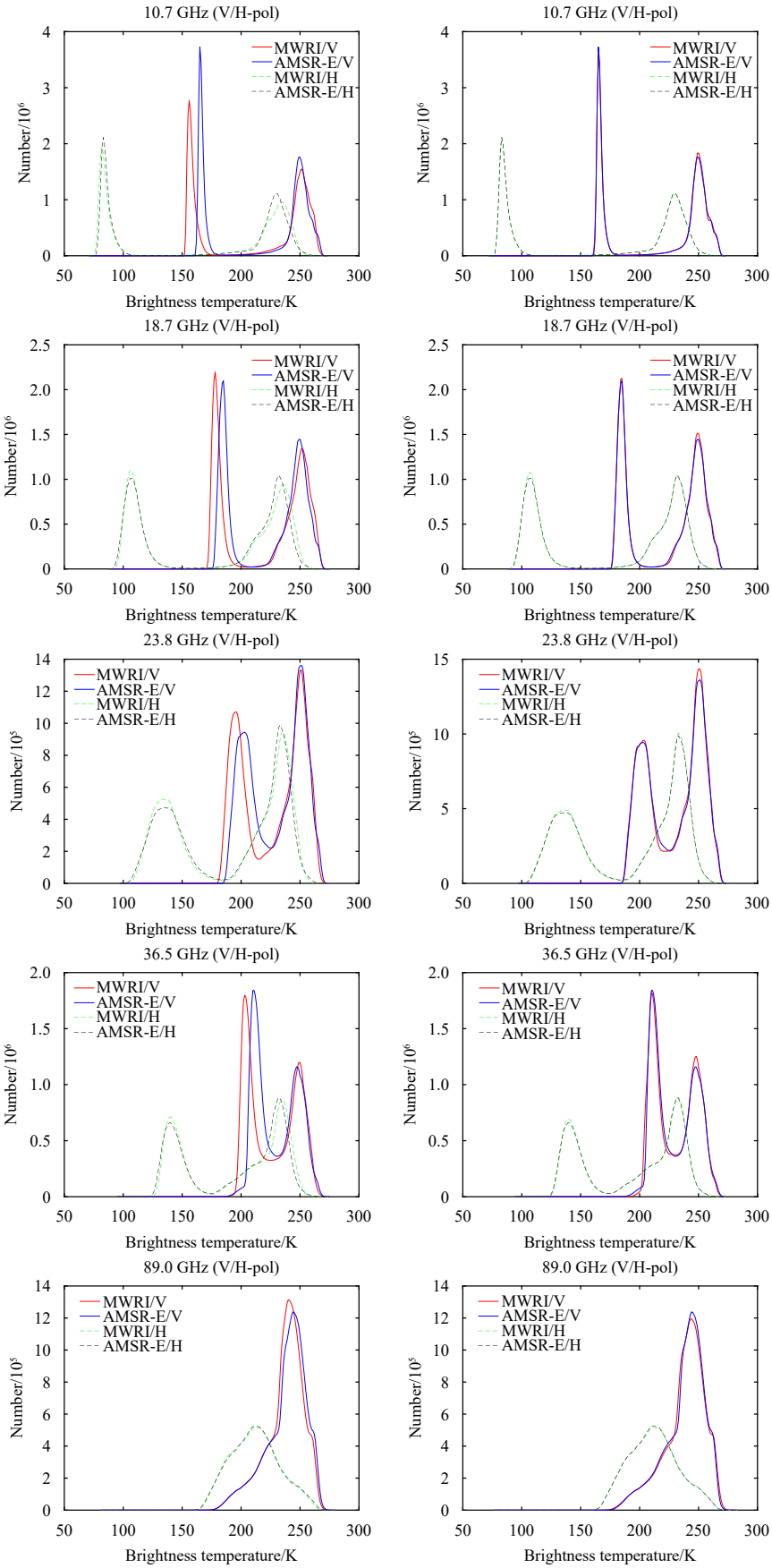

Fig. 2. Statistical histograms of data on T_b of the MWRI and AMSR-E (before and after calibration) for all channels with H/V polarization (left: original MWRI and AMSR-E; right: corrected MWRI and AMSR-E).

calibration were significantly reduced, except for those for the channel at 89.0 GHz. The STD and RMSE values of the other channels ranged from 1.59 K to 2.57 K, and 1.64 K to 2.68 K, respectively. In general, the cross-calibration method used here was effective at cross-calibrating the data on the daily average T_b of the MWRI.

Furthermore, the two corresponding jumps in the results of calibration marked in Fig. 4 were analyzed. Observational data from the FY-3B MWRI were adjusted on May 25, 2011, and led to uncertainty errors between the MWRI and the AMSR-E data. In addition, the corresponding jump positions of the data were related to the seasonal characteristics of the Arctic, and were affected by the changes in the physical marine processes during the periods of the formation and melting of the sea ice. As shown in Fig. 5, the ratios of the water, ice, and ice-water mixture were calculated based on the sea ice concentration (SIC) from the AMSR-E L3 data provided by the NSDIC. As described in Section 3.1.1, the edges of the sea ice detected using the T_b polarization ratios of the MWRI (Zhang, 2012) were similar to the results obtained for the ice and water boundaries of the AMSR-E L3 SIC value 15 as threshold. Massom et al. (1998) divided the ice and water according to the SIC threshold of 75. Here, 15 and 75 were

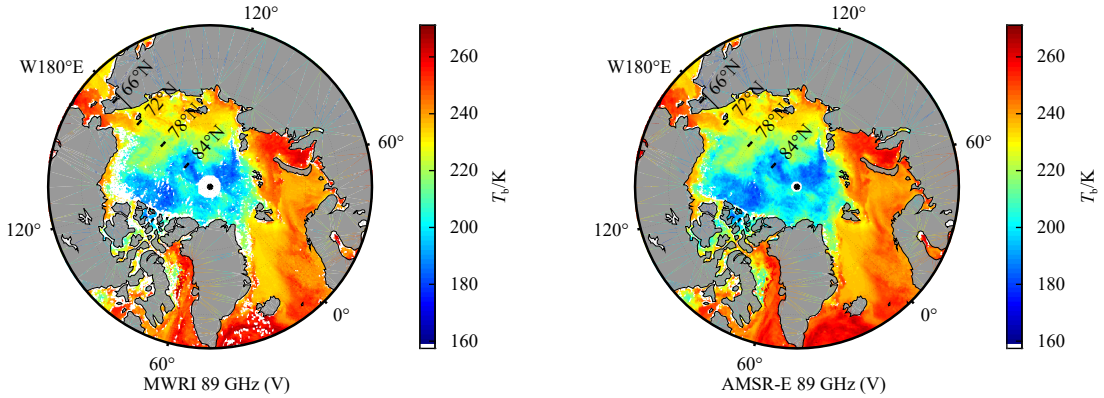

Fig. 3. Comparison of daily average values of T_b for the MWRI and AMSR-E (V polarization 89 GHz, on January 1, 2011).

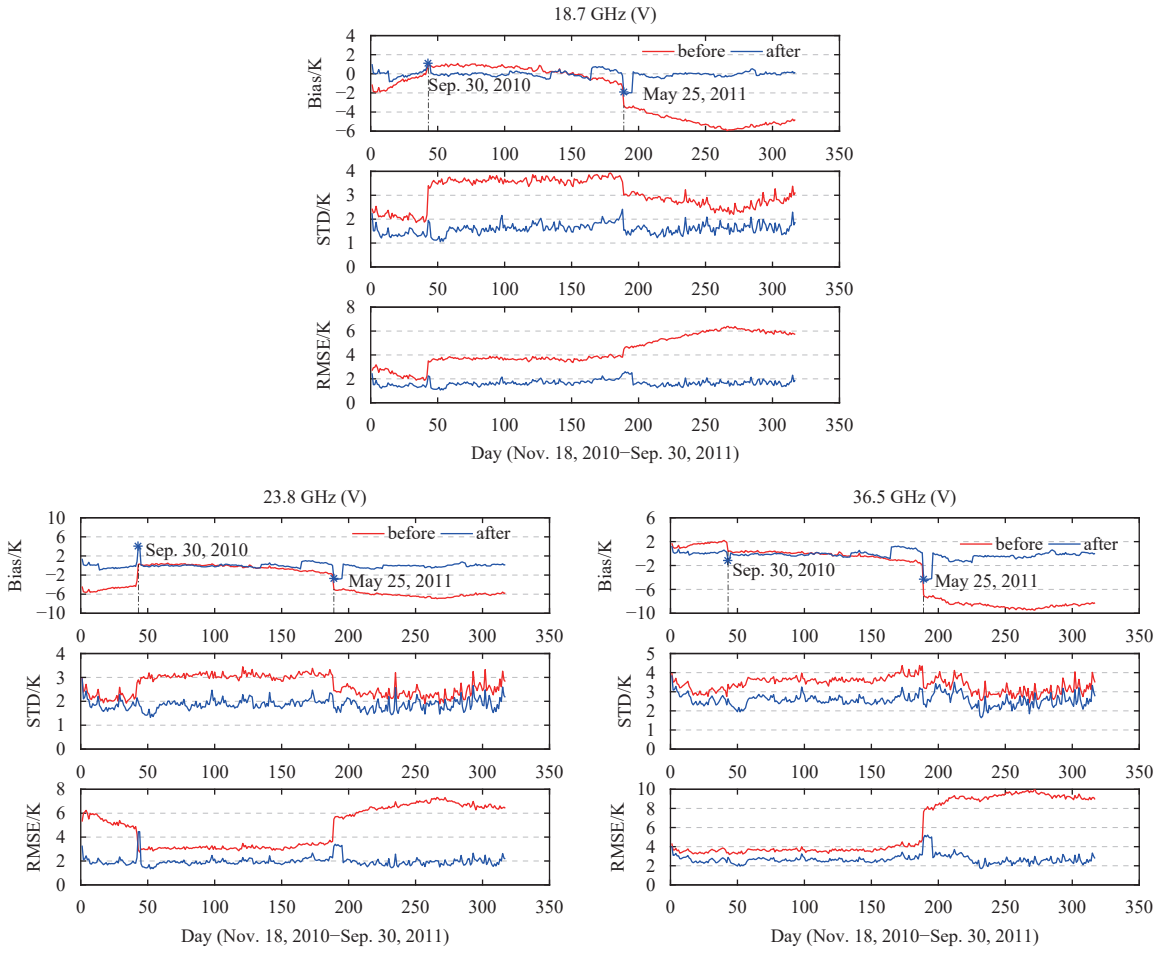

Fig. 4.

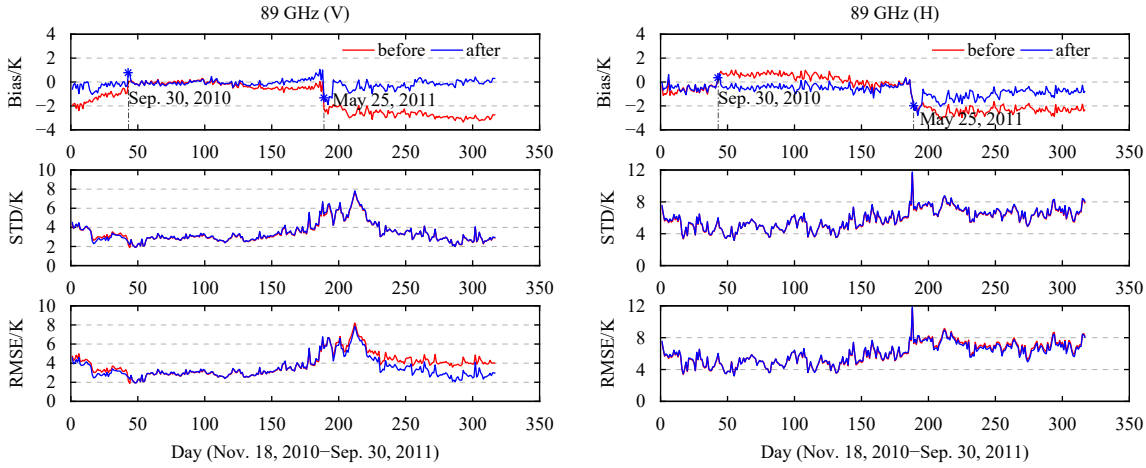

Fig. 4. Comparison of the biases, STD, and RMSE in terms of values of T_b between the MWRI and the AMSR-E (channels: V18.7 GHz, V23.8 GHz, V36.5 GHz, H/V 89.0 GHz), before and after cross calibration.

Table 3. Comparison of statistical parameters before and after cross-calibration between the MWRI and AMSR-E in terms of data on the daily average T_b

Channel	Frequency/ GHz	Before cross-calibration/ after cross-calibration		
		Bias/K	STD/K	RMSE/K
V	18.7	–1.98/–0.06	3.06/1.59	4.33/1.64
V	23.8	–3.27/–0.07	2.68/1.87	4.82/1.96
V	36.5	–3.40/–0.24	3.38/2.57	5.90/2.68
V	89.0	–1.39/–0.16	3.41/3.44	3.84/3.46
H	89.0	–0.90/–0.71	5.82/5.90	6.00/5.96

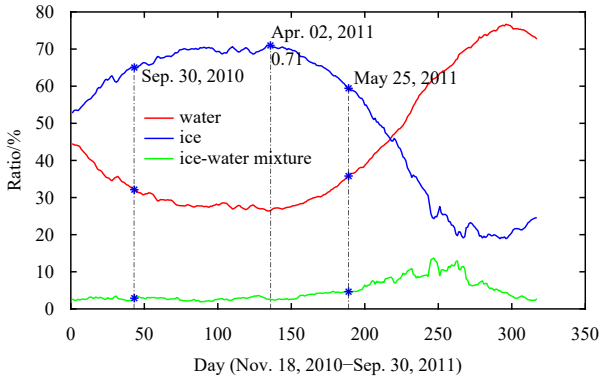

Fig. 5. Ratios of the water, ice, and ice-water mixture in the Arctic.

used as thresholds. The SIC values greater than 75% is ice, those smaller than 15% is sea water, and the rest represent areas of ice-water mixtures.

In the Arctic, the annual sea ice forms from October to December every year, and its extent gradually increases from January to March, reaching its maximum in March and early April. Figure 5 shows that the ratio of sea ice on April 2 reached 71%. The trend of variation in the sea ice was opposite to that of the sea water. December 30 marked the beginning of the growth of sea ice, and May 25 was marked the seasonal ice melt after the sea ice had reached its maximum extent. The distributions of bias, STD, and RMSE in Fig. 4 (especially in channels V18.7 GHz, 23.8 GHz, and 36.5 GHz) show the trends of change above two jump points. The differences in T_b between the MWRI and the AMSR-E were affected by the seasonal changing of sea ice due to its formation and melting. The annual and seasonal regularities of the influence of this on the calibration data will be further studied for other sensors in future research.

4.2.2 *Snow-depth comparison*

The daily snow depths based on the algorithm described in Section 3.2 were averaged by a 5-d sliding window to reduce noise (Li et al., 2019). From January 1 to April 30, 2011, the 5-d average values of snow depth were derived from the FY-3B/MWRI brightness temperatures before and after the cross-calibration to the baseline of the AMSR-E in the overlapping periods.

As an example, in Fig. 6, the distributions of snow depth derived from the MWRI before and after cross-calibration show similar spatial characteristics to those of the AMSR-E level 3 products on February 5, 2011. The areas in white indicate the missing data and abnormal points, and those in black represent snow depths greater than 50 cm. Multi-year sea ices, in light-gray, represents water in the open sea areas, and the dark gray represents land. The valid values were 0–50 cm as shown in the figures with the colored bars.

Figure 7 is a comparison of the daily snow depths, which shows that the relevant brightness temperatures of the MWRI after cross-calibration were closer to those of the AMSR-E L3 products. The distribution of the histogram of the snow depth biases, and the mean absolute error (MAE) between the MWRI and the AMSR-E L3 products before and after cross-calibration, are shown in Figs 8–9. As shown in the histogram (Fig. 8), after cross-calibration, the differences between the datasets were generally symmetrically distributed around a central value of 0 cm. More than 99% of the biases were concentrated between ±20 cm. The histogram of biases and the MAE values in Figs 8–9 show that the results of snow depths retrieval according to values of T_b of the MWRI were more consistent with those of the AMSR-E than the results before calibration.

Furthermore, the monthly snow depths obtained by the calibrated MWRI, and the differences between this and the results of the AMSR-E L3, were studied to evaluate the effects of cross-calibration as shown in Table 4. Following cross-calibration, the biases in monthly snow depths were in the range 0.18–0.38 cm, the standard deviation ranged from 4.19 cm to 4.80 cm, and the RMSE ranged from 4.19 cm to 4.81 cm.

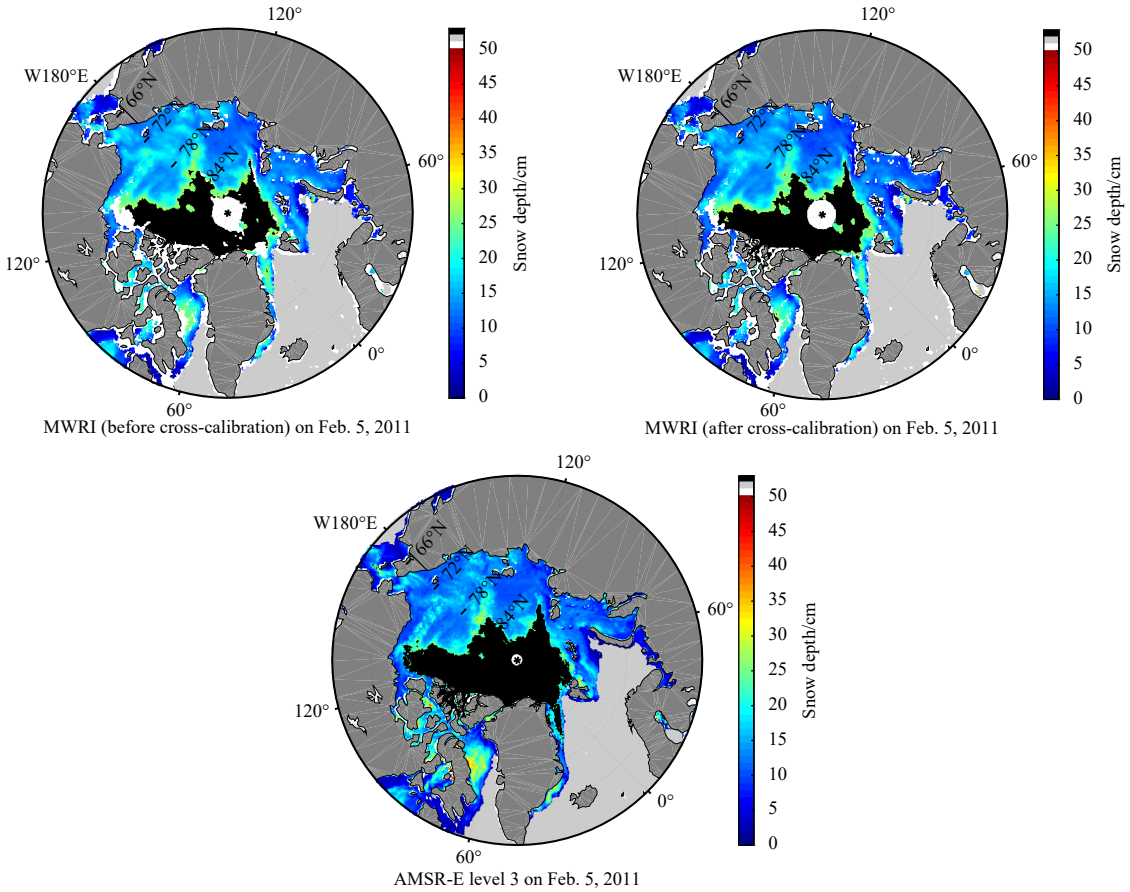

Fig. 6. Comparison of distributions of snow depth derived from the MWRI before and after cross-calibration, and those of the AMSR-E level 3 in the Arctic.

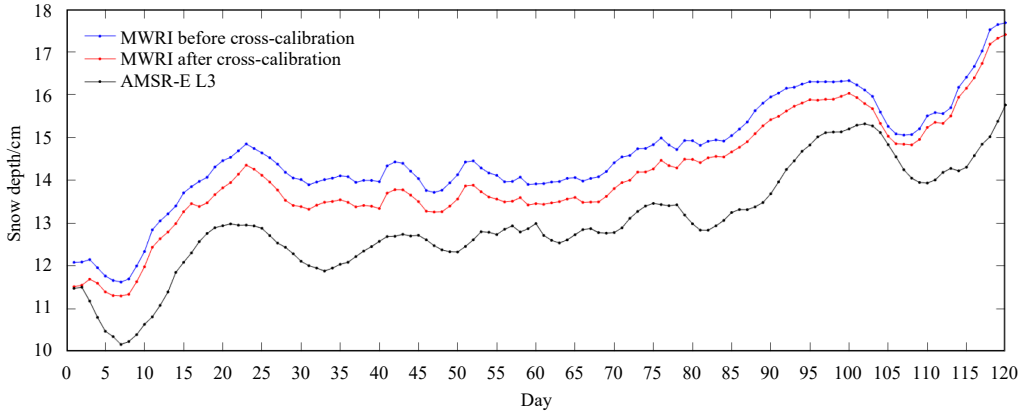

Fig. 7. Comparison of snow depth obtained by the MWRI and AMSR-E L3 from January 1 to April 30, 2011 (120 d).

5 Conclusions

This study calibrated data on the monthly Arctic brightness temperature (T_b) obtained by the MWRI and the AMSR-E from November 18, 2010 to September 30, 2011. The method used was shown to be useful for the cross-calibration of values of T_b of the MWRI as well as the subsequent measurement of snow depths on seasonal ice in the Arctic. Some deviations were observed between the MWRI and the AMSR-E T_b data from scatters of the monthly T_b and its daily data distributions, but a clear consistency and linear relationship was noted between the sensors. Using robust linear regression, parameters of the monthly cross-calibration were obtained at all five frequencies (10.7 GHz, 18.7 GHz, 23.8 GHz, 36.5 GHz, and 89.0 GHz), dual polarization (H, V), and ascending and descending orbits for the two sensors. Statistical analysis was carried out to evaluate the performance of the results of cross-calibration of the matching datasets. Following cross-calibration, all channels of the MWRI and the AMSR-E data were corrected. The MWRI T_b data were optimized using the cross-calibration method. Furthermore, the cross-calibration parameters were applied to data of the daily T_b of the channels, including V18.7 GHz, V23.8 GHz, and V36.5 GHz as well as H/V 89.0 GHz, to calculate snow depths on seasonal sea ice in the Arc-

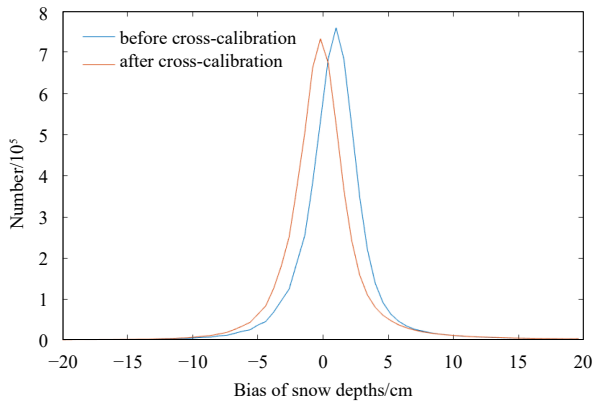

Fig. 8. The histogram of snow depth biases between the MWRI (before and after cross-calibration) and AMSR-E data from January 1 to April 30, 2011

tic. The parameters of monthly cross-calibration were effective in correcting the daily data on T_b, although there was a certain deviation in the results for snow depth retrieval. Compared with those of the AMSR-E L3 product, the results were significantly closer to the AMSR-E data than those before cross-calibration, and the bias was significantly reduced. The research in the paper can provide parameter-related support for the application of T_b data of the MWRI from the Arctic.

The instrument-related parameters of the MWRI and AMSR-E are similar, but there are certain differences in their ground resolutions and angles of incidence. The seasonal change in sea ice during the formation and melting periods also affected the results of the cross-calibration between the sensors. These aspects will be investigated further to reduce the differences between their results. Future work will involve an examination of the MWRI data of the FY-3 satellite series, seasonal characteristics of the MWRI as yielded by cross-calibration, and the use of cross-calibration to the inversion of the parameters of snow and ice in the Arctic.

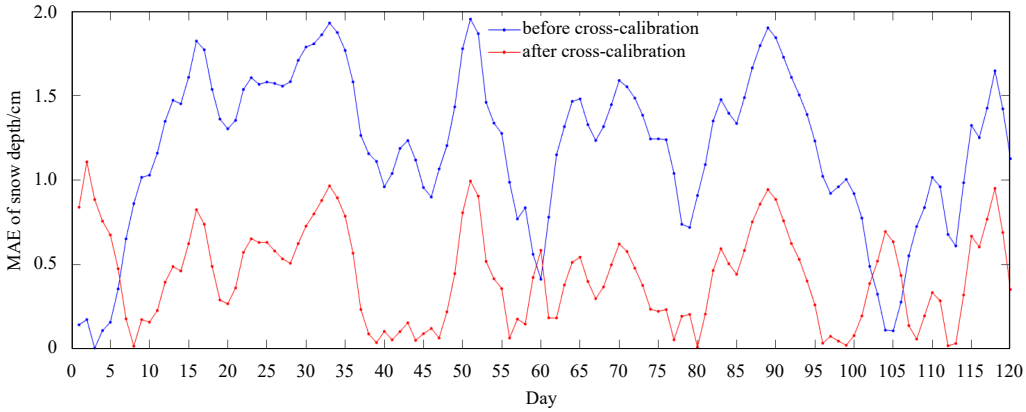

Fig. 9. The Mean absolute error (MAE) of snow depths between the MWRI results and the AMSR-E L3 products from January 1 to April 30, 2011 (120 d).

Table 4. Monthly statistical evaluation of differences in snow depth between the MWRI and the AMSR-E L3 after cross-calibration

Time	Number	Bias/cm	STD/cm	RMSE/cm
Jan. 2011	1 317 171	0.25	4.80	4.81
Feb. 2011	1 374 930	0.31	4.59	4.60
Mar. 2011	1 554 678	0.38	4.57	4.59
Apr. 2011	1 448 672	0.18	4.19	4.19

Acknowledgements

The MWRI data were provided by the NSMC Satellite Data Center, and the AMSR-E data were provided by the DAAC of NASA at the American National Snow and Ice Data Center.

References

Abdalati W, Steffen K, Otto C, et al. 1995. Comparison of brightness temperatures from SSMI instruments on the DMSP F8 and FII satellites for Antarctica and the Greenland ice sheet. International Journal of Remote Sensing, 16(7): 1223–1229, doi: 10.1080/01431169508954473

Cavalieri D J, Comiso J, Markus T. 2014. AMSR-E/Aqua Daily L3 12.5 km Brightness Temperature, Sea Ice Concentration, & Snow Depth Polar Grids, Version 3. Boulder, Colorado USA: NASA National Snow and Ice Data Center Distributed Active Archive Center

Cavalieri D J, Parkinson C L. 2012. Arctic sea ice variability and trends, 1979–2010. The Cryosphere, 6: 881–889, doi: 10.5194/tc-6-881-2012

Cavalieri D J, Parkinson C L, DiGirolamo N, et al. 2012. Intersensor calibration between F13 SSMI and F17 SSMIS for global sea ice data records. IEEE Geoscience and Remote Sensing Letters, 9(2): 233–236, doi: 10.1109/LGRS.2011.2166754

Cavalieri D J, Parkinson C L, Vinnikov K Y. 2003. 30-year satellite record reveals contrasting Arctic and Antarctic decadal sea ice variability. Geophysical Research Letters, 30(18): 1970

Chander G, Hewison T J, Fox N, et al. 2013. Overview of intercalibration of satellite instruments. IEEE Transactions on Geoscience and Remote Sensing, 51(3): 1056–1080, doi: 10.1109/TGRS.2012.2228654

Comiso J C, Cavalieri D J, Markus T. 2003. Sea ice concentration, ice temperature, and snow depth using AMSR-E data. IEEE Transactions on Geoscience and Remote Sensing, 41(2): 243–252, doi: 10.1109/TGRS.2002.808317

Comiso J C, Parkinson C L, Gersten R, et al. 2008. Accelerated decline in the Arctic sea ice cover. Geophysical Research Letters, 35(1): L01703

Das N N, Colliander A, Chan S K, et al. 2014. Intercomparisons of brightness temperature observations over land from AMSR-E and WindSat. IEEE Transactions on Geoscience and Remote Sensing, 52(1): 452–464, doi: 10.1109/TGRS.2013.2241445

Derksen C, Walker A E. 2003. Identification of systematic bias in the cross-platform (SMMR and SSM/I) EASE-grid brightness tem-

perature time series. IEEE Transactions on Geoscience and Remote Sensing, 41(4): 910–915, doi: 10.1109/TGRS.2003.812003

Du Jinyang, Kimball J S, Shi Jiancheng, et al. 2014. Inter-calibration of satellite passive microwave land observations from AMSR-E and AMSR2 using overlapping FY3B-MWRI sensor measurements. Remote Sensing, 6(9): 8594–8616, doi: 10.3390/rs6098594

Gao Shuo, Li Zhen, Chen Quan, et al. 2019. Inter-sensor calibration between HY-2B and AMSR2 passive microwave data in land surface and first result for snow water equivalent retrieval. Sensors, 19(22): 5023, doi: 10.3390/s19225023

Hu Tongxi, Zhao Tianjie, Shi Jiancheng, et al. 2016. Inter-calibration of AMSR-E and AMSR2 brightness temperature. Remote Sensing Technology and Application (in Chinese), 31(5): 919–924

Huang Wei, Hao Yanling, Wang Jin, et al. 2013. Brightness temperature data comparison and evaluation of FY-3B microwave radiation imager with AMSR-E. Periodical of Ocean University of China (in Chinese), 43(11): 99–111

Jezek K C, Merry C J, Cavalieri D J. 1993. Comparison of SMMR and SSM/I passive microwave data collected over Antarctica. Annals of Glaciology, 17: 131–136, doi: 10.3189/S0260305500012726

Kaleschke L, Lüpkes C, Vihma T, et al. 2001. SSM/I sea ice remote sensing for mesoscale ocean-atmosphere interaction analysis. Canadian Journal of Remote Sensing, 27(5): 526–537, doi: 10.1080/07038992.2001.10854892

Kelly R E, Chang A T, Tsang L, et al. 2003. A prototype AMSR-E global snow area and snow depth algorithm. IEEE Transactions on Geoscience and Remote Sensing, 41(2): 230–242, doi: 10.1109/TGRS.2003.809118

Li Lele, Chen Haihua, Guan Lei. 2019. Retrieval of snow depth on sea ice in the arctic using the FengYun-3B microwave radiation imager. Journal of Ocean University of China, 18(3): 580–588, doi: 10.1007/s11802-019-3873-y

Li Qin, Zhong Ruofei. 2011. Multiple surface parameters retrieval of simulated AMSR-E data. Remote Sensing for Land and Resources (in Chinese), 23(1): 42–47

Liu Qingquan, Ji Qing, Pang Xiaoping, et al. 2018. Inter-calibration of passive microwave satellite brightness temperatures observed by F13 SSM/I and F17 SSMIS for the retrieval of snow depth on Arctic first-year sea ice. Remote Sensing, 10(1): 36

Lu Zhou, Stroeve J, Xu Shiming, et al. 2020. Inter-comparison of snow depth over sea ice from multiple methods. The Cryosphere Discussions, preprint, https://doi.org/10.5194/tc-2020-65

Markus T, Cavalieri D J. 1998. Snow depth distribution over sea ice in the Southern Ocean from satellite passive microwave data. In: Jeffries M O, ed. Antarctic Sea Ice: Physical Processes, Interactions and Variability. Washington, DC: American Geophysical Union, 19–40

Markus T, Cavalieri D J. 2008. AMSR-E algorithm theoretical basis document supplement: Sea ice products. Greenbelt, MD, USA: Hydrospheric and Biospheric Sciences Laboratory, NASA Goddard Space Flight Center, 1–9

Maslowski W, Kinney J C, Higgins M, et al. 2012. The future of arctic sea ice. Annual Review of Earth and Planetary Sciences, 40(1): 625–654, doi: 10.1146/annurev-earth-042711-105345

Massom R A, Harris P T, Michael K J, et al. 1998. The distribution and formative processes of latent-heat polynyas in East Antarctica. Annals of Glaciology, 27: 420–426, doi: 10.3189/1998AoG27-1-420-426

Meier W N, Khalsa S J S, Savoie M H. 2011. Intersensor calibration between F-13 SSM/I and F-17 SSMIS near-real-time sea ice estimates. IEEE Transactions on Geoscience and Remote Sensing, 49(9): 3343–3349, doi: 10.1109/TGRS.2011.2117433

Nihashi S, Ohshima K I, Tamura T, et al. 2009. Thickness and production of sea ice in the Okhotsk Sea coastal polynyas from AMSR-E. Journal of Geophysical Research, 114(C10): C10025, doi: 10.1029/2008JC005222

Parkinson C L, Cavalieri D J. 2008. Arctic sea ice variability and trends, 1979–2006. Journal of Geophysical Research: Oceans, 113(C7): C07003

Spreen G, Kaleschke L, Heygster G. 2008. Sea ice remote sensing using AMSR-E 89-GHz channels. Journal of Geophysical Research: Oceans, 113(C2): C02S03

Stroeve J, Maslanik J, Li Xiaoming. 1998. An intercomparison of DMSP F11- and F13-derived sea ice products. Remote Sensing of Environment, 64(2): 132–152, doi: 10.1016/S0034-4257(97)00174-0

Svendsen E, Kloster K, Farrelly B, et al. 1983. Norwegian remote sensing experiment: Evaluation of the nimbus 7 scanning multichannel microwave radiometer for sea ice research. Journal of Geophysical Research: Oceans, 88(C5): 2781–2791, doi: 10.1029/JC088iC05p02781

Yang Hu, Weng Fuzhong, Lv Liqing, et al. 2011. The FengYun-3 microwave radiation imager on-orbit verification. IEEE Transactions on Geoscience and Remote Sensing, 49(11): 4552–4560, doi: 10.1109/TGRS.2011.2148200

Yang Hu, Zou Xiaolei, Li Xiaoqing, et al. 2012. Environmental data records from FengYun-3B microwave radiation imager. IEEE Transactions on Geoscience and Remote Sensing, 50(12): 4986–4993, doi: 10.1109/TGRS.2012.2197003

Zhang Shugang. 2012. An algorithm to detect arctic sea ice edge using microwave brightness temperature. Periodical of Ocean University of China (in Chinese), 42(11): 1–7